Characteristic Impedance and Propagation of the First Higher Order Microstrip Mode in Frequency and Time Domain

Shyue-Dar Chen, *Member, IEEE,* and Ching-Kuang C. Tzuang, *Fellow, IEEE*

***Abstract*—This paper experimentally and theoretically confirms the validity of the definition proposed by Das for computing the complex characteristic impedance of the first higher order (EH_1) microstrip mode. The normalized complex propagation constant and complex characteristic impedance of the microstrip obtained by the rigorous full-wave integral-equation method is also presented. To better understand the circuit behavior of the leaky mode at the respective frequencies, the results are analyzed in both frequency and transformed steepest descent plane. A differential time-domain reflectometry (TDR) experiment shows that the experimental results are in excellent agreement with the time-domain plots obtained theoretically by the inverse discrete Fourier transform of the transmission line modeled by the dispersive characteristic. The propagation characteristics of the echoed signals in the time domain, which are reflected from the open end of the leaky line, are analyzed in detail using the corresponding group velocity of the EH_1 mode. The wide spread of the echoed signals in the time domain is the direct result of the highly dispersive group velocity. The slowest group velocity is in the leaky region. The time-to-frequency conversion of the measured TDR data reveals that the reflection, leaky, and propagation zones coexist simultaneously for the EH_1 mode propagation. The conversion also accurately assesses the attenuation constant of the EH_1 mode if the attenuation is not too high. The Fourier transform of the TDR responses also simultaneously yields the input reflection coefficient (S_{11}) and the complex characteristic impedance. The complex characteristic impedance extracted from the TDR responses also agrees closely with the theoretical data.**

***Index Terms*—Group velocity leaky waves, impedance measurement, microstrip, time-domain reflectometry.**

I. Introduction

NEW LEAKY- and surface-wave effects in various planar and nonplanar guiding structures have been reported for applications in microwave integrated circuits and devices. The undesired spurious coupling caused by leaky effects may stem from dominant-mode leakage in stripline with an air gap [1], additional leaky dominant mode [2], [3], and conductor-backed slotline [4]. The physical interpretation and discussion of these effects can facilitate new methods for suppressing the leakage effects, such as using shorting pins [5] and changing the packaging or geometric parameters of the guiding structures [6], [7]. However, exciting a leaky mode in a controllable fashion is also very important for practical use of the leaky lines. Menzel successfully designed a leaky-wave antenna in a microstrip by properly exciting the first higher order mode via step discontinuities, matching circuits, and a mode suppressor [8]. Furthermore, excitation of microstrips first and second higher order modes using composite microslotline and microcoplanar waveguide (micro-CPW) structures, respectively, has exhibited very good relative power absorbed (RPA) value (typically greater than 90%) and excellent input matching (typically a reflection coefficient smaller than -15 dB) of the leaky lines [9], [10].

To excite the leaky lines properly, the layout for the three-dimensional (3-D) structure is usually optimized by adjusting the geometrical parameters through a lengthy process that is based on only limited knowledge of the complex propagation constant of the targeted leaky mode [11]. Consequently, the issue of the optimal feeding structures for exciting a specific leaky line arises. To resolve this issue, the assessment of the leaky-mode excitation embedded in the complicated radiation process, which also involves space waves and surface waves, mandates appropriate methods for extracting the leaky modes' contribution [10], [12], [13]. In addition to the quantitative assessment, the characteristic impedance of a leaky line provides an insightful circuit-domain view of the leaky line, thus enabling the design of an optimal feeding network. Given the propagation constant and characteristic impedance of the leaky line, the microwave circuit description and modeling of the guiding structure are fulfilled [14]. Das demonstrated that a 3-D circuit comprised of short-circuit slotline stubs could be modeled accurately with a one-dimensional leaky line when the leaky mode dominates in the microwave circuit [4]. He defined the characteristic impedance (Z_c) for a leaky strip-type line using the following expression:

$$Z_c = \frac{P_b}{|I_t|^2} = \frac{\frac{1}{2}\int_S da\hat{z} \cdot (\vec{E} \times \vec{H}^*)_{\text{excluding leaky fields}}}{|I_t|^2} \tag{1}$$

where I_t denotes the total modal currents and P_b represents the bound-field portion of the Poynting power, excluding the exponentially growing parts of the leaky field in the modal solution of the leaky mode. Das referred to the leaky fields as being only loosely attached to the central guiding region that are responsible for distributed radiation loss. Thereby the leaky-fields are not associated or are only loosely associated with the circuit

Manuscript received June 15, 1999; revised January 12, 2001.

The authors are with the Institute of Electrical Communication Engineering, National Chiao Tung University, Hsinchu, Taiwan, R.O.C. (e-mail: cktzuang@cc.nctu.edu.tw).

Publisher Item Identifier S 0018-9480(02)04049-8.

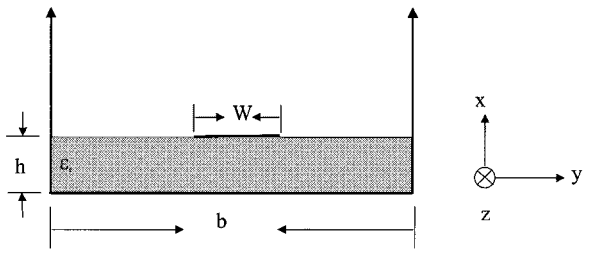

Fig. 1. General microstrip line and coordinate system. The Z-axis is along the microstrip line. The structural parameters are used through this paper. The two sidewalls are separated with a distance b in the y-direction.

element in a circuit sense. Unless the complex characteristic impedance is experimentally verified, as with the microstrip bound mode, doubts still remain about employing the complex characteristic impedance for circuit simulation.

In addition to the presentation of complex characteristic impedance obtained theoretically using (1) for the first higher order mode of a microstrip line, this study applies an experimental setup based on the differential time-domain reflectometry (TDR) to: 1) excite the first higher order odd mode of the microstrip; 2) theoretically and experimentally explore the corresponding time-domain propagation characteristics; 3) relate the group velocity of the odd-mode propagation to the time-domain step response; 4) interpret the broad-band time-domain propagation characteristics; and 5) confirm the validity of the definition for complex characteristic impedance. This approach obtains a clear and comprehensive circuit level picture of the first higher order microstrip mode.

II. Characteristic Impedance of the Microstrip's First Higher Order Mode

The structural parameters of the microstrip line shown in Fig. 1 are applied here for analyses and experiments. The microstrip with a width of 16 mm is printed on a 30-mil-thick ($h = 0.762$ mm) ULTRALAM substrate of $\varepsilon_r = 2.55$ and the sidewall distance b is set at 480 mm (30 W in Fig. 1). The microstrip is parallel to the z-axis, which is normal to the transverse xy-plane.

Numerous previous investigations have reported the full-wave two-dimensional (2-D) modal analyses of strip-type transmission lines. In general, the procedures for obtaining the characteristic impedance using 2-D modal analyses closely resemble each other [15]. The first step is to determine the propagation constant, from which the currents on the strip are then obtained. Next, the Poynting power is computed using the cross-sectional electrical and magnetic fields derived from the known current distributions on the strip. For clarity, Appendix A briefly summarizes the formulation. Cautions should be exercised when calculating the transverse fields in the case of the leaky line, and the exponentially growing components in the total field expression of the transverse plane should be

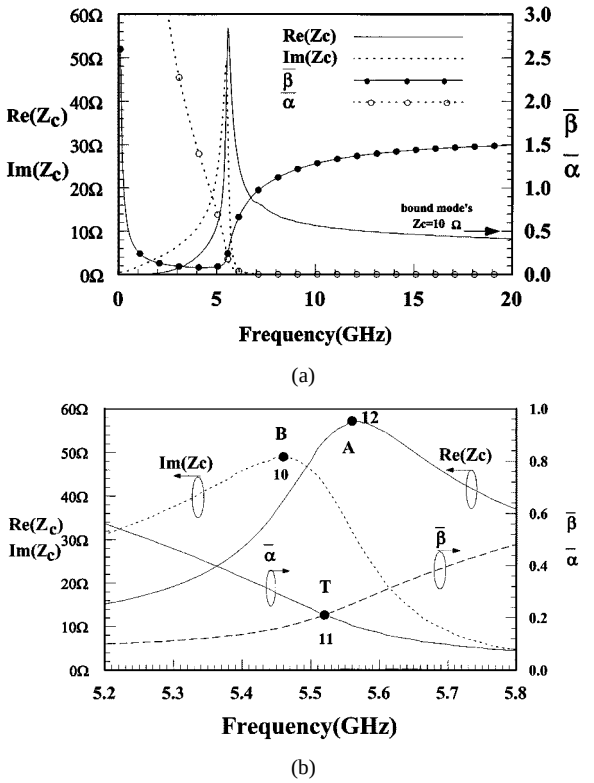

Fig. 2. (a) Normalized propagation constant and complex characteristic impedance of the first higher order microstrip mode. The characteristic impedance of dominant mode is slightly dispersive, approximate 10 Ω. (b) Enlargement of the frequency scales on the summit region.

excluded. For example, the E_y-component of the TE mode with respect to the x-axis is expressed as follows:

$$E_y(x,y) = \frac{-j}{b}\sum_{m=m_b}^{m_t}\frac{(2-\delta_{m0})}{2k_{x2}\left(\gamma^2+k_y^2\right)} \cdot \left(1+\tilde{R}_{21}^{\mathrm{TE}}\right)e^{-jk_{x2}(x-h)}\cos(k_y y) \cdot \left(\gamma^2\int_{\mathrm{strip}} J_y\cdot\cos(k_y y')\,dy' - jk_y\gamma\int_{\mathrm{strip}} J_z\cdot\sin(k_y y')\,dy'\right). \quad (2)$$

Given a leaky-mode solution, the bound field of a leaky mode is the summation of the harmonic terms from m_b to m_t, where m_t is the upper limit for truncating the infinite series and m_b is the first term of the bound field. The magnitude of the generalized reflection coefficient $(\tilde{R}_{21}^{\mathrm{TE}}(m))$ must be less than one to ensure the term is bound field [see Appendix A for the expression of $\tilde{R}_{21}^{\mathrm{TE}}(m)$]. For $m = 0, 1, 2, \ldots, m_b - 1$, $|\tilde{R}_{21}^{\mathrm{TE}}(m)|$ are more than one, representing the leaky field of the leaky mode and suggesting the mathematical condition for the improper physical solution. Recent investigations of such leaky modes that are improper (they do not satisfy the radiation condition at infinity, but are physically significant) used the semianalytical 3-D Green's function to obtain the excitation amplitude of a leaky mode [12], [13].

TABLE I

Point	Frequency(GHz)	β/k_o	α/k_o
D	7.22880	0.9999962	0.2201984E-05
A	7.22896	1.000000	0.2288161E-06

Brews explicitly shows that the characteristic impedance is complex whenever the propagation constant is also complex [16, eqs. (13) and (14)]. Fig. 2(a) plots the normalized complex propagation constant ($\overline{\gamma}$) of the first higher order (EH_1) mode using the vertical scales on the right axis ($\overline{\gamma} = \overline{\beta} - j\overline{\alpha}$, $\overline{\beta} = \beta/k_0$, $\overline{\alpha} = \alpha/k_0$; k_0 is the free-space wavenumber). The real and imaginary parts of the complex characteristic impedance [$\mathrm{Re}(Z_c)$ and $\mathrm{Im}(Z_c)$], obtained by the procedure described earlier, are superimposed in Fig. 2, with scales on the left-hand-side axis. Fig. 2(b) presents the expanded view of Fig. 2(a), in the frequency range from 5.2 to 5.8 GHz, for a detailed investigation of leaky properties. Notably, two conducting sidewalls, separated by a distance b, are placed along the y-direction in Fig. 1, thus rendering the application of the discrete Fourier series. Extensive numerical analysis reveals that when b exceeds 30× the microstrip width (30 W), the sidewalls have negligible influence on the propagating characteristics of the leaky line. The dispersion curves and complex characteristic impedance converge with an error of less then 2%.

The onset frequency of the leaky mode is at approximately 7.2 GHz, above which the normalized phase constant ($\overline{\beta}$) is greater than one and the normalized attenuation constant ($\overline{\alpha}$) is negligible for the particular case study. The so-called spectral-gap region must reside around the onset frequency [17]. Appendix B gives the expression for estimating the bandwidth of the spectral gap using the available dispersion data at and below the onset frequencies (see F_A and F_C). Since the spectral-gap region manifests nonphysical solutions for the propagation constants, the estimated bandwidth of the spectral gap is important here. Notably, the measured (dispersive) propagation constants in the spectral gap are often obscure, mainly because of the radiation in the form of a surface or space wave from the exciting source in the spectral-gap region [18]. This implies that the spectral gap will significantly impact the circuit modeling of the leaky EH_1 mode from the characteristic impedance point of view. The normalized leakage constant at the onset frequency F_A is 0.23×10^{-6}(see Table I). Appendix B reveals that the bandwidth of the spectral gap is approximately the ratio of $\overline{\alpha}$ to S, where S is the slope of the normalized phase constant at the onset frequency F_A. Detailed analyses in Appendix B indicate that the spectral gap is only approximately 10-kHz wide, too small to be plotted and distinguishable in Fig. 2(a). Since the spectral gap is very small, it is thus negligible in our analysis. Furthermore, the Tektronix CSA803A differential TDR test system has a sampling period of 1.0 ps and 5120 points in the maximum record length. These parameters are equivalent to having a best frequency resolution of approximately 100 MHz in the spectrum, which is not fine enough to discriminate the circuit effect of the spectral gap in our case study.

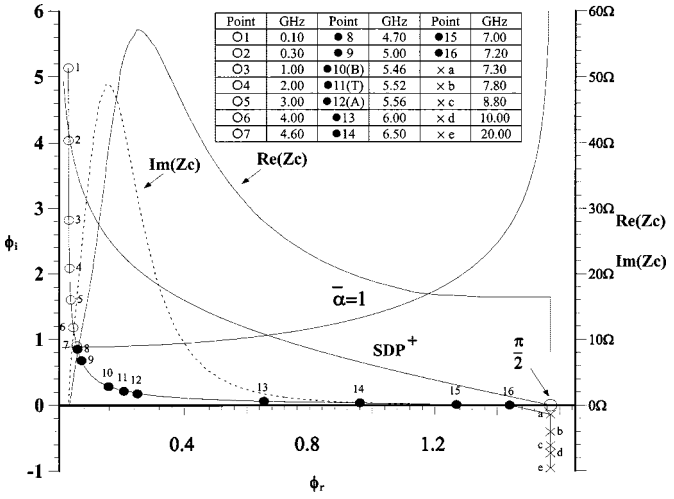

Fig. 3. Complex characteristic impedance of the EH_1 microstrip mode and the locations of the leaky pole are imposed on the transformed ϕ-plane (steepest descent plane). A transformation $\gamma = \beta - j\alpha = k_o \sin(\phi)$ $k_x = \sqrt{k_o^2 - \gamma^2} = k_o \cos(\phi)$ is used where $\phi = \phi_r - j\phi_i$ is the complex plane. The curve labeled as SDP^+ is the steepest descent path through the saddle point $\phi_r = \pi/2$. The leaky poles within the region under the curve SDP^+ and curve $\overline{\alpha} = 1$ $(\cos(\phi_r)\sinh(\phi_i) = \overline{\alpha} = 1)$ contribute strongly to the far field. The symbols ○ and • represent the leaky pole locations that $\overline{\alpha} > 1$, $\overline{\alpha} < 1$, respectively. The symbol × represents the bound (real) pole locations. The list of specific frequencies corresponding to the numerical and alphabetical points is also tabulated.

If the frequency is increased further, to well above the onset frequency, the value of $\overline{\beta}$ will asymptotically approach that of the dominant bound (even) mode. As expected, we observe the corresponding Z_c of the EH_1 mode, which is real and nearly reaches that of the bound mode.

Below the onset frequency, the EH_1 mode becomes leaky, with its attenuation constant increasing as the frequency decreases. As illustrated on summit A and B in Fig. 2(b), the maximum values of $\mathrm{Re}(Z_c)$ and $\mathrm{Im}(Z_c)$ are 56.8 (summit A) and 48.8 Ω (summit B) at 5.56 and 5.46 GHz, respectively. Furthermore, let the intersecting point of curves $\overline{\beta}$ and $\overline{\alpha}$ be point T at approximately 5.52 GHz. Below T, $\overline{\alpha}$ increases rapidly and $\mathrm{Re}(Z_c)$ quickly declines to zero. However, $\mathrm{Im}(Z_c)$ rises sharply from nearly zero to summit B and then gradually declines to zero again. Consequently, we can observe that the leaky line, in the leaky region, depicts a strong reactive (inductive) circuit behavior below T and becomes lossy above T. As in Fig. 2(a), the frequency below summit B, $\mathrm{Re}(Z_c)$, and $\mathrm{Im}(Z_c)$ is approximately 0.08 and 1.8 Ω, respectively, at 1.0 GHz, implying the leaky line is essentially a short circuit. The combined effect of large inductance near and below point T and the short-circuit behavior below summit B means the leaky mode is not easily excited below point T. The above finding correlates with the finding of Lee [19] and Oliner in that, for large decay rates ($\overline{\alpha} > 1$), the contribution of the leaky mode to the total field can usually be disregarded. To clarify this phenomenon, Fig. 3 superimposes the complex characteristic impedance of the various leaky poles onto the steepest descent plane. Twenty leaky poles in the steepest descent plane are numbered and listed in the inset of Fig. 3. A transformation $\gamma = \beta - j\alpha = k_o \sin(\phi)$ is applied where $\phi = \phi_r - j\phi_i$ is the complex plane. The first

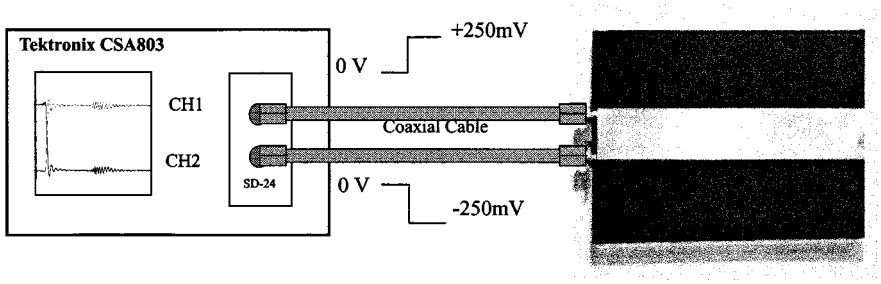

Fig. 4. Differential TDR experimental setup for exciting purely odd mode and investigating the propagating properties of the first higher order microstrip mode. (*left-hand side*) Tektronix CSA803A with a sampling head SD-24. (*right-hand side*) Microstrip line under test.

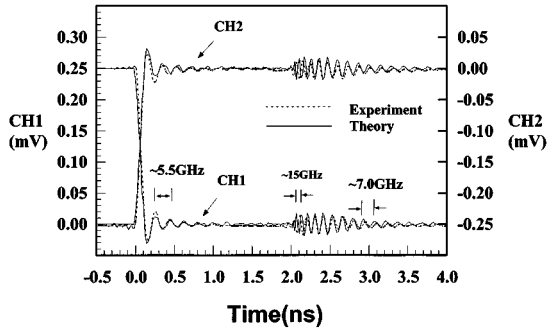

Fig. 5. Experimental and theoretical differential TDR step responses of the microstrip. The theoretical step response in the time domain is obtained by the inverse direct Fourier transform of the transmission line modeled by the complex propagation constant and complex characteristic impedance of Fig. 2. $CH1$ is the positive-going step voltage, displaying TDR voltage 0∼500 mV and corresponding to reflection coefficient $\rho = -1 \sim \rho = +1$. Similarly, $CH2$ is the negative-going step voltage, displaying TDR voltage $0 \sim -500$ mV and corresponding to reflection coefficient $\rho = -1 \sim \rho = +1$. The differential TDR responses of the microstrip: measurement (- - -) and theory (—).

seven points, denoted by the symbol ◯, located below 4.6 GHz, are the leaky poles outside the curve $\overline{\alpha} = 1$, and simultaneously display almost short circuit behavior; $\mathrm{Re}(Z_c)$ and $\mathrm{Im}(Z_c)$ rapidly drop from 10 Ω to 0. The short-circuit property makes the excitation of the first seven leaky poles extremely difficult. Points 8–16, denoted by "•," are leaky poles within the region bounded by the curves SDP^+ and $\overline{\alpha} = 1$. The curve labeled SDP^+ represents the steepest descent path through the saddle point $\phi_r = \pi/2$. Notice that points 10–12 correspond to summit B, point T, and summit A, respectively. Points 8–11 define a region where complex characteristic impedance is highly dispersive, and where a strongly inductive component such as $\mathrm{Re}(Z_c)$ rapidly falls to zero. Such large reactive components tend to prohibit the leaky mode from being excited. Points 12–16, above point T, constitute the leaky-mode region of the relatively insignificant $\mathrm{Im}(Z_c)$, thus defining a region that exhibits strong leakage if excited properly. Meanwhile, points a–c, marked with symbol ×, are classified as real poles that propagate in the form of the bound mode, also possess real characteristic impedance.

III. Differential TDR Experimental Setup

As shown in Fig. 4, a differential TDR experiment is conducted to validate the power–current definition for the characteristic impedance of the leaky mode. Using the Tektronix CSA803A communication analyzer, a pair of differential step voltages with a rise time of 17.5 ps are inflicted into the left-hand side (source terminal) of a 178-mm-long microstrip line. Thus, the differential step voltages naturally excite the odd mode of the microstrip. Fig. 5 displays the measured differential TDR step responses. The positive-going step waveform travels along a short 50-Ω coaxial cable labeled from −0.5 to 0 ns and experiences a short-circuit load, thus swinging from $\rho = 0$ (250 mV) to $\rho = -1$ (0 mV). On the contrary, the negative-going step swings from $\rho = 0$ (−250 mV) to $\rho = -1$ (0 mV). Two interesting time-domain propagation characteristics merit further investigation. First, an exponentially decaying and oscillating waveform of resonant frequency near 5.5 GHz is observed between 0–2.0 ns. As soon as the differential step voltage waves enter the microstrip and generate the decayed resonance close to point T (point 11 at 5.52 GHz) implies that the leaky mode at summit A is largely excited because its characteristic impedance is close to the 50-Ω reference load. Second, the returned signals from the open end, starting from 2.0 ns, show that the frequencies within the signals exceed 5.5 GHz, more precisely above the onset frequency of 7.2 GHz. This phenomenon implies that the energy of the leaky mode is almost exhausted during the round-trip as the step voltage waves return to the source end. The qualitative description of the measured time-domain responses agrees well with expectations based on the theoretical data from Section II.

IV. Time-Domain Analysis

The step responses in the time domain can be recovered from the dispersive characteristics reported in Section II, namely, the propagation constant and complex characteristic impedance. If the input step waveforms are truly differential, only the odd mode is excited in the microstrip with an open end as a load. Thus, the electrical wall may be placed at the center of the microstrip and the entire experimental setup can be modeled by a half-circuit, as illustrated in Fig. 6, where V_s denotes the positive-going step voltage source of 17.5-ps rise time, and R_s represents the internal referenced impedance (typically 50 Ω). The complex propagation constant, complex characteristic impedance, and length L together model the microstrip that propagates the EH_1 mode and is terminated by an open end. Herein, the effective positions of the junction of the SMA connector are located on the differential TDR measurement, as shown in Fig. 6. The measured maximum reflection coefficient (Γ_g) is 0.020 and 0.012 for $CH1$ and $CH2$, respectively. The different values appear to result from the soldering or variation

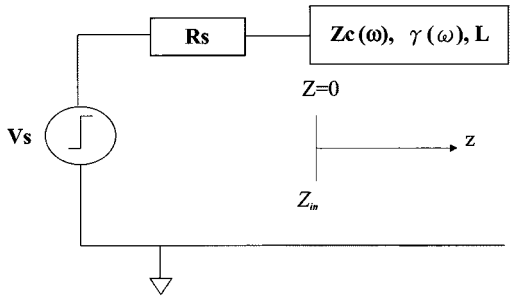

Fig. 6. Equivalent circuit representation of the TDR experiment on the step response for a microstrip leaky mode. Vs is the positive-going waveform with 500-mV step voltage and 17.5-ps rise time.

of the separate SMA connector. Since the reflection coefficient is very small, the effect of the coaxial-to-microstrip transition can be neglected in our analyses of the TDR waveforms. The time–harmonic terminal voltage at $z = 0$ (the source end) can be expressed as

$$V_o(\omega) = \frac{Z_{in}(\omega)}{Z_{in}(\omega) + R_s} V_s(\omega) = \frac{1}{2}(1 + S_{11})V_s(\omega) \quad (3)$$

where S_{11} denotes the reflection coefficient at the source end, assuming that the reference impedance is R_s; $V_s(\omega)$ represents the time–harmonic component of the step voltage waveform, and $Z_{in}(\omega)$ is the input impedance looking into the leaky line. Applying the transmission-line equation, $Z_{in}(\omega)$ becomes

$$Z_{in}(\omega) = -jZ_c(\omega)\cot(\gamma L). \quad (4)$$

Finally, the step response is obtained by the inverse discrete Fourier transformation of $V_o(\omega)$. As shown in Fig. 5, the theoretical differential TDR responses of the microstrip are superimposed onto the measured data. Excellent agreement exists between the two sets of data, although a small discrepancy is observed for the returned signals near 2.0 ns. Since the theoretical TDR responses virtually duplicate the measured results, the characteristic impedance reported in Section II is verified. Consequently, further time-domain investigation of the EH_1-mode propagation becomes meaningful. Closely examining the TDR response reveals that in the echoed (returned) signals between 2.0–4.0 ns, the high-frequency signals arrive earlier than the lower ones. Fig. 7 validates this observation. By computing the normalized group velocity [V_g/c; $V_g = (\partial\omega/\partial\beta)$, c is the speed of light] using the data shown in Fig. 2(a), Fig. 7 shows that the minimum group velocity occurs near 5.58 GHz, which is slightly higher than summit A. Above 5.58 GHz, the group velocity increases from $0.155c$ to the asymptotic limit of $0.605c$. Notably, the group velocity is below the speed of light. The figure also presents the phase constant (β), not normalized to k_0, to better relate the phase constant and group velocity. Below 5.58 GHz, β is small and nearly independent of frequency. However, the group velocity cannot be approximated by taking the first-order derivative of the $\omega - \beta$ diagram [22] and, thus, the upper limit at which V_g/c is equal to unity is imposed in Fig. 7.

Time (τ_d) required for the voltage wave to travel from the source end back to the original position is

$$\tau_d = \frac{2L}{V_g}. \quad (5)$$

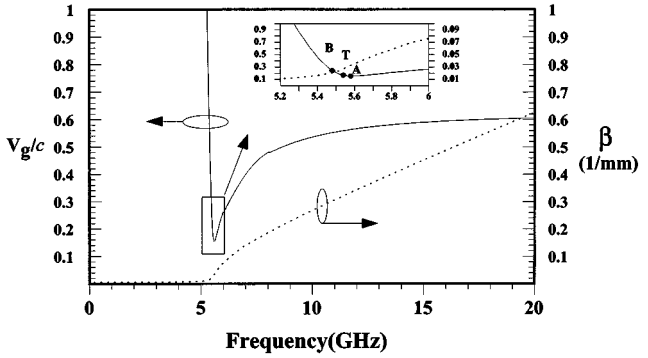

Fig. 7. Phase constant (β) and normalized group velocity (V_g/c) of the first higher order microstrip mode ($h = 30$ mil, $w = 16$ mm, $\varepsilon_r = 2.55$).

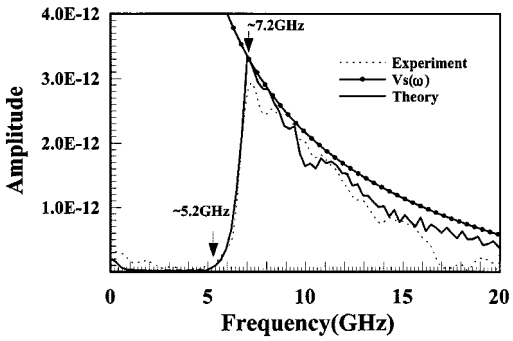

Fig. 8. Amplitude spectra for analyzing signals contained in the wavepacket. The gating signals are between 2.0–4.0 ns. $V_s(\omega)$ is the time–harmonic component of the step waveform with 17.5-ps rise time and 500-mV step voltage.

The group velocity at 7.0 and 15.0 GHz is $0.40c$ and $0.59c$, respectively. Meanwhile, the corresponding delay times are 2.967 and 2.01 ns, as clearly displayed in Fig. 5. The echoed signals that return from the microstrip open end are spread out. The 15.0-GHz signal component travels at a higher group velocity and returns to the source end approximately 2 ns after the step voltage waveform is inflicted. Meanwhile, the 7.0-GHz signal component, which is in the leaky-mode region, travels at a lower group velocity, thus appearing approximately 1 ns later than the 15.0-GHz signal.

V. Frequency-Domain Analysis

The signals in the wavepacket (from 2.0 to 4.0 ns) are analyzed using experimental and theoretical data by the discrete fast Fourier transformation (DFFT). Fig. 8 illustrates the relationship between the amplitude and frequency of the computed spectra. Amplitudes below 5.2 GHz are close to zero, clearly indicating that signals below 5.2 GHz (near point 9) are hard to propagate. This phenomenon agrees with the implication in Fig. 3 that signals below point 7 (4.6 GHz) can be disregarded. Such signals can be disregarded because the complex characteristic impedance is nearly zero, thus reflecting most signals below point 8 back to the source end. Fig. 8 also plots $V_s(\omega)$, the Fourier transform of the step waveform (500 mV in amplitude, 17.5 ps in rise time). Above 7.2 GHz, which is the onset frequency of the leaky EH_1 mode (Fig. 3, point 16), both experimental and theoretical values closely follow the $V_s(\omega)$ curve with little discrepancy. Therefore, by only propagating the EH_1

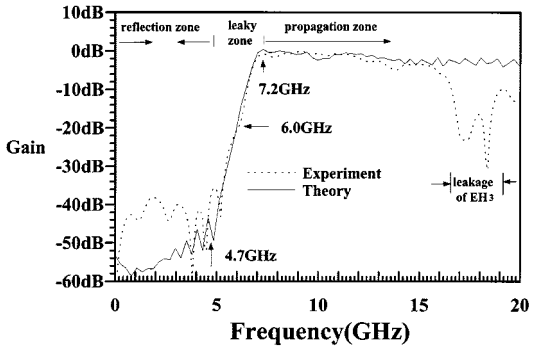

Fig. 9. Experimental and theoretical voltage gain $(V_o(\omega)/V_s(\omega))$ defined as the time–harmonic component of the echoed signals to that of the step voltage.

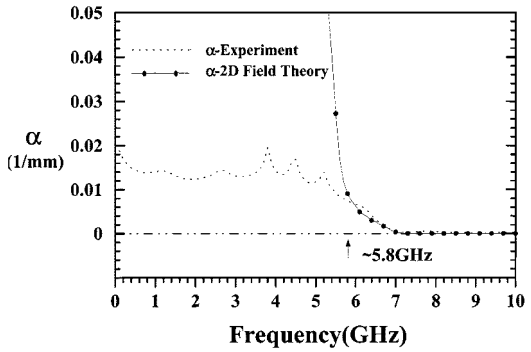

Fig. 10. Comparison of the attenuation constants obtained by differential TDR experiment and the 2-D field theory. Noticed that α is not normalized to k_0. The experimental data is obtained from the gain of Fig. 9 by (9).

mode, the microstrip line acts as a high-pass filter with corner frequency at the onset frequency. Lying between 7.2–5.2 GHz is the leaky region excited by the differential step voltage waves. Notably, the DFFT gating process causes a residual value at zero frequency (dc). For an open microstrip line, the highly leaky region of the third higher order (EH_3) mode lies at approximately the triple frequency of the EH_1 mode [23]–[25]. Meanwhile, the EH_3 mode (also an odd mode) can be excited by the differential TDR apparatus. The loss displayed in Fig. 8 between 16.0–20.0 GHz [figures that are nearly three times 5.46 (point 10) and 6.5 GHz (point 14)] is closely associated with the leakage of the EH_3 mode. The voltage gain $G(\omega)$ is defined as the ratio of the time–harmonic components of the echoes to $V_s(\omega)$ written as

$$G(\omega) = \frac{\text{DFFT(Echoed Signals)}}{V_s(\omega)}. \tag{6}$$

Fig. 9 plots $G(\omega)$, and clearly reveals three propagating zones for the EH_1 mode. Below 4.7 GHz, the theoretical (experimental) data show a reduced gain approximately -50-dB (-40-dB) gain reduction, confirming that only a very small portion of the signal can propagate below point 8 in Fig. 3 This region is thus designated as a reflection zone. Above 7.2 GHz, both the theoretical and experimental gain curves approach 0 dB, indicating that a high-pass propagating zone exits. The gain plot between 5.2–7.2 GHz quantifies how the leaky mode gets excited and survives the round-trip leakage. Near 7.2 GHz (point 16 of Fig. 3), the leaky mode exhibits nearly zero attenuation constant [see Fig. 2(a)] and, thus, a gain reduction of nearly 0 dB is observed in Fig. 9. Meanwhile, at 6.0 GHz (near point 9 of Fig. 3), the leaky mode has an attenuation constant of 0.05 k_0 and experiences a reduction of -20 dB in the round-trip, closely approaching the predicated value of -19.5 dB, computed by

$$G_{\text{dB}}\Big|_{\text{leaky zone}} = 20 \cdot \log_{10} e^{-2\alpha L}. \tag{7}$$

Fig. 10 compares the computed attenuation constant using (7) and the theoretical data shown in Fig. 2. Excellent agreement is obtained with small values [from 0$\sim$0.007 (1/mm)] for the attenuation constant between 5.8–7.2 GHz. The sensitivity of the TDR scope prohibits accurate assessment of the larger attenuation constant and, thus, Fig. 10 shows a growing discrepancy in the attenuation constant below 5.8 GHz. Shortening the leaky line used to measure large attenuation constants is one way to enhance the accuracy of the measurement.

Finally, an attempt is made to extract complex characteristic impedance from time-domain differential TDR waveforms. The terminal voltage of (3) is expressed in terms of multiple reflections in the transmission line as [26]

$$V_0(\omega) = \frac{Z_c V_s(\omega)}{Z_c + R_s}\Big[1 + \rho_l e^{-2\gamma L} + \rho_l \rho_s e^{-2\gamma L} + \rho_l e^{-2\gamma L}\big(\rho_l \rho_s e^{-2\gamma L}\big) + \cdots\Big] \tag{8}$$

where ρ_l and ρ_s denote the reflection coefficients at the source and load terminals, respectively. The terminal voltage $V_0(\omega)$ before the first round-trip reflection wave arrives at the source end can be reduced to

$$V_0(\omega) = V_s(\omega)\frac{Z_c}{Z_c + R_s}. \tag{9}$$

Equation (9) simulates the case of an infinitely long transmission line. In practice, as long as the returned signals do not interfere with the transient signals that have sufficient time to settle. Fig. 5 shows that the transient signals decay to become negligible before the returned signals arrive at the source end at 2.0 ns. The reflection coefficient and the characteristic impedance can thus be obtained from the terminal voltage by

$$S_{11} = \frac{Z_c - R_s}{Z_c + R_s} = 2\frac{V_0(\omega)}{V_s(\omega)} - 1 \tag{10}$$

$$Z_c = R_s \frac{V_0\big(\omega/V_s(\omega)\big)}{1 - V_0\big(\omega/V_s(\omega)\big)} \tag{11}$$

where $V_0(\omega)$ is the discrete Fourier transform, using the gating transient voltage waveform between 0–2.0 ns and then padding with zero above 2.0 ns. Thus, the reflection coefficient S_{11} is obtained. Fig. 11 plots the input reflection coefficient in decibels, including both its real and imaginary parts. The figure also contains the numeral points of Fig. 3. Notably, points 10 (summit B), 11 (point T), and 12 (summit A) show that $\text{Re}(S_{11})$ and $\text{Im}(S_{11})$ are near zero, displaying good input matching to 50 Ω between points 10 and 13. Detailed observation reveals that the minimum of $|S_{11}|$ is approximately -15.6 dB at 5.75 GHz. Between points 11 and 13, $|S_{11}|$ is below -10 dB, indicating

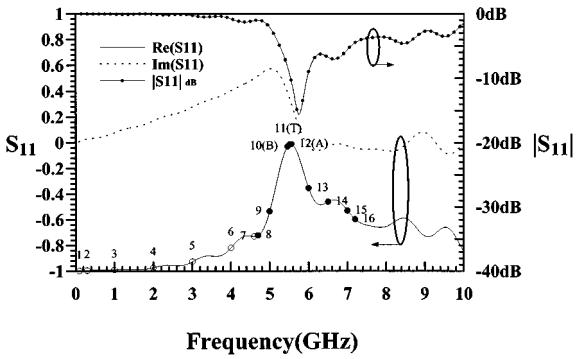

Fig. 11. Reflection coefficient S_{11} obtained from the TDR data by (10) using the gating experimental data from 0 to 2.0 ns. The numerals shown in the plot follow the inset of Fig. 3.

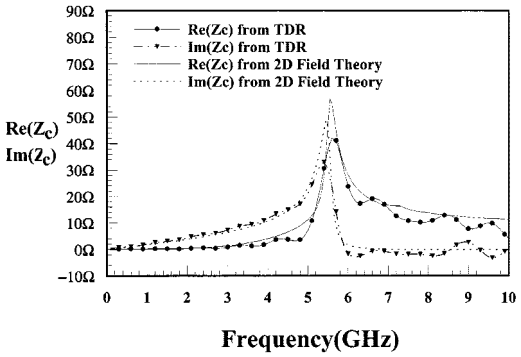

Fig. 12. Comparison of the complex characteristic impedance obtained both from theory and experiment that are computed by (1) and (11).

that this region is easily excited by the present apparatus. Points 1–7 are outside the $\overline{\alpha} = 1$ curve, as shown in Fig. 3. Notably, applying $1 - |S_{11}|^2$ estimates that significant electromagnetic energy enters the transmission line when using the present experimental apparatus, specifically, 6.5% at 3.0 GHz (point 5) and 21% at 4.6 GHz (point 7). The reflection zone reported in Fig. 9 actually comprises a transitional region between the reflection and leaky zones. Fig. 12 compares the directly extracted complex characteristic impedance of the EH_1 mode using (11) and the theoretical data obtained by (1), clearly showing excellent agreement between the theoretical and experimental data. The differential TDR experiment, through (11), confirms that the complex characteristic impedance of the EH_1 mode has an inductive (resistive) component that peaks at summit B (A) or point 10 (12) of Fig. 2(a). The discrepant peak values at summits A and B are caused by truncating the infinite oscillation.

VI. Conclusions

This study has experimentally and theoretically confirmed the definition proposed by Das [4] for obtaining the complex characteristic impedance of a leaky line by a case study of the first higher order (EH_1) microstrip mode. The EH_1 microstrip mode may propagate in three types of zones in the broad-band spectra, namely, the propagation, leaky, and reflection zones. In the propagation zone, where the slow wave propagates with zero attenuation, the propagation constant and characteristic impedance are both real. The leaky zone enters below the

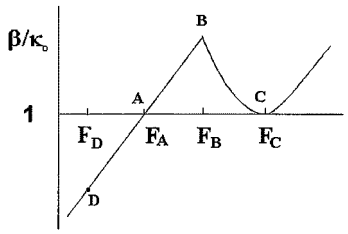

Fig. 13. Typical transition region of the spectral gap. The normalized dispersion curves are divided into three regions. The right of point C, where the real spectral solution touches one, is the bound-wave region and is physical. The left of point A, which is the complex solution, is the leaky-wave region and is physical. Between the leaky- and bound-wave regions is the so-call spectral gap, where solutions are nonphysical.

propagation zone, showing the complex propagation constant and the complex characteristic impedance. The complex characteristic impedance is close to 50 Ω, together with a large inductive part, implying that the leaky-mode antenna of this type is usually easy to match to 50 Ω. The group velocity is lowest in the leaky region, falling to approximately $0.155c$ (c: the speed of light) at 5.58 GHz in this particular case study. Although the phase velocity exceeds c in the leaky zone, the group velocity is smaller than c.

Below the leaky zone is the reflection zone, where complex characteristic impedance falls into two regions. The first region contains complex characteristic impedance of nearly zero (near 3.0 GHz, $\overline{\alpha} = 2.4$ for the particular case study), representing a short-circuit phenomenon. Meanwhile, the second region is characterized by characteristic impedance with a small real part, but a growing imaginary (inductive) part, with the imaginary part growing with frequency. Such inductive circuit loading closely reflects the EH_1 mode launched from the differential TDR heads, thus creating a transitional region (between 3.0–4.6 GHz in the particular case study) transforming the pure reflection zone into a leaky zone.

The complex characteristic impedance, combined with the complex propagation constant of the EH_1 mode, explicitly explains the propagation characteristics of the three zones associated with the differential step excitation of a long leaky line. The proposed differential TDR test method consists of time-domain signals in two parts. The first part involves the transient waveforms instantly reflecting at source end. Meanwhile, the second part is focused on the signals returning from the open end. The transient signals are shown to be associated with the input reflection coefficient (S_{11}) and complex characteristic impedance of the leaky line. On the other hand, the echoed signals are related to the leaky and propagation zones, from which the attenuation (leaky) constant can be accurately extracted.

Appendix A
2-D Dyadic Green's Function

Assume that the time–harmonic dependence is $e^{j\cdot\varpi\cdot t}$ and the guided-wave z-dependant solution is $e^{-j\cdot\gamma\cdot z}$. What follows is the 2-D dyadic Green's function applied in the integral-equation formulation for obtaining the leaky-mode solution, as shown at the bottom of the following page.

A more detailed derivation is referred to in [27]and [28].

APPENDIX B
ESTIMATION OF SPECTRAL-GAP BANDWIDTH

The bandwidth of the spectral gap can be related to the leaky constant α at point A and the slope of line segment AB by estimating the phase constant at point B in terms of the leaky constant α at point A and assuming that the wavenumber between points A and B is linear. What follows is parallel to the work of [17], except the explicit mathematical expression relating the bandwidth of the spectral gap to the leakage attenuation constant.

According to Fig. 13, the propagation constant is near unity in the spectral gap. The leaky field propagates in the parallel-plate form. Thus, we can set $k_y = 0$, and the Helmholtz relation is reduced to

$$k_0^2 = k_z^2 + k_x^2. \tag{A-1}$$

The direction of x is parallel to the parallel plates. Herein, k_z and k_x are defined in terms of their real and imaginary parts as follows:

$$k_z = \beta - j\alpha \tag{A-2}$$

$$k_x = \beta_x - j\alpha_x. \tag{A-3}$$

By normalizing k_z and k_x with respect to k_0, substituting (A-2) and (A-3), into (A-1), and separating the real and imaginary parts, we obtain

$$1 = \overline{\beta}^2 - \overline{\alpha}^2 + \overline{\beta}_x^2 - \overline{\alpha}_x \tag{A-4}$$

$$\overline{\alpha}\overline{\beta} = -\overline{\alpha}_x\overline{\beta}_x. \tag{A-5}$$

$$\begin{aligned}
&\overline{\overline{G}}_e^{(2,2)} \\
&= -\frac{1}{k^2}\,\delta(x-x')\,\delta(y-y')\hat{x}\hat{x} + \frac{-j}{b}\sum_{m=0}^{\infty}\frac{(2-\delta_{m0})}{2k_{x2}(\gamma^2+k_y^2)} \\
&\cdot\begin{bmatrix} 0 & 0 & 0 \\ 0 & \gamma^2\cos(k_y y)\cos(k_y y') & -jk_y\gamma\cos(k_y y)\sin(k_y y') \\ 0 & jk_y\gamma\sin(k_y y)\cos(k_y y') & k_y^2\sin(k_y y)\sin(k_y y') \end{bmatrix}\left(1+\tilde{R}_{21}^{TE}\right)e^{-jk_{x2}(x-h)} + \frac{-j}{b}\sum_{m=1}^{\infty}\frac{1}{k_{x2}(\gamma^2+k_y^2)} \\
&\cdot\begin{bmatrix} \frac{k_{x2}k_y(\gamma^2+k_y^2)}{k_2^2}\sin(k_y y)\sin(k_y y') & \frac{jk_{x2}k_y(\gamma^2+k_y^2)}{k_2^2}\sin(k_y y)\cos(k_y y') & -\frac{k_{x2}k_y(\gamma^2+k_y^2)}{k_2^2}\sin(k_y y)\sin(k_y y') \\ \frac{-jk_{x2}k_y(\gamma^2+k_y^2)}{k_2^2}\cos(k_y y)\sin(k_y y') & \frac{k_{x2}^2k_y^2}{k_2^2}\cos(k_y y)\cos(k_y y') & \frac{jk_{x2}^2k_y\gamma}{k_2^2}\cos(k_y y)\sin(k_y y') \\ \frac{k_{x2}\gamma(\gamma^2+k_y^2)}{k_2^2}\sin(k_y y)\sin(k_y y') & -\frac{jk_{x2}^2k_y\gamma}{k_2^2}\sin(k_y y)\cos(k_y y') & \frac{k_{x2}^2\gamma^2}{k_2^2}\sin(k_y y)\sin(k_y y') \end{bmatrix} \\
&\cdot\begin{bmatrix} \left(1-\tilde{R}_{21}^{TM}\right) \\ \left(1+\tilde{R}_{21}^{TM}\right) \\ \left(1+\tilde{R}_{21}^{TM}\right) \end{bmatrix} e^{-jk_{x2}(x-h)}
\end{aligned}$$

$$\tilde{R}_{21} = \frac{R_{21}+R_{10}e^{-2jk_{x1}h}}{1+R_{21}R_{10}e^{-2jk_{x1}h}}$$

$$\tilde{R}_{21} \in \left(\tilde{R}_{21}^{TE},\, \tilde{R}_{21}^{TM}\right)$$

$$R_{21} \in \left(R_{21}^{TE},\, R_{21}^{TM}\right)$$

$$R_{10} = \begin{cases} -1, & \text{TE mode} \\ 1, & \text{TM mode} \end{cases}$$

$$R_{21}^{TE} = \frac{\mu_1 k_{x2} - \mu_2 k_{x1}}{\mu_1 k_{x2} + \mu_2 k_{x1}}$$

$$R_{21}^{TM} = \frac{\varepsilon_1 k_{x2} - \varepsilon_2 k_{x1}}{\varepsilon_1 k_{x2} + \varepsilon_2 k_{x1}}$$

$$k_{xl}^2 = (\varepsilon_l \varepsilon_0 k_0)^2 - \gamma^2 - k_y^2$$

$$k_y = \frac{m\pi}{b}, \qquad l = 1, 2$$

$$\delta_{m0} = \begin{cases} 1, & m = 0 \\ 0, & m \neq 0 \end{cases}$$

At point A, $\overline{\beta}$ is unity. Solving (A-4) and (A-5), at point A, we have

$$\left(\overline{\beta}_x^2\right)_A = \frac{\overline{\alpha}^2 \pm \sqrt{\overline{\alpha}^4 + 4\overline{\alpha}^2}}{2}. \tag{A-6}$$

Since, in our case, $\overline{\alpha} \ll 1$, $\overline{\alpha}^4 \ll \overline{\alpha}^2 \ll \overline{\alpha}$. By selecting the "+" sign in (A-6), we obtain

$$\left(\overline{\beta}_x\right)_A \approx \left(\sqrt{\overline{\alpha}}\right)_A \tag{A-7}$$

$$\left(\overline{\alpha}_x\right)_A \approx \left(-\sqrt{\overline{\alpha}}\right)_A. \tag{A-8}$$

As pointed out in [17], from points A to B, $\overline{\alpha}_x$ is constant while $\overline{\beta}_x$ becomes smaller. At point B, $\alpha = 0$, β, and α_x are nonzero, and $\beta_x = 0$ from (A-5). We solve (A-4) and get

$$\left(\overline{\beta}\right)_B = \sqrt{1 + \left(\overline{\alpha}_x^2\right)_B} \approx 1 + \frac{1}{2}\left(\overline{\alpha}_x^2\right)_B. \tag{A-9}$$

Since $(\overline{\alpha}_x)_B = (\overline{\alpha}_x)_A = (-\sqrt{\overline{\alpha}})_A$, (A-9) is reduced to

$$\left(\overline{\beta}\right)_B \approx 1 + \frac{1}{2}\left(\overline{\alpha}\right)_A. \tag{A-10}$$

Assuming that the wavenumber between points A and B depict a straight line, AB is linear in this range. Thus, the expression relating to the bandwidth of the spectral gap and the leakage constant at point A is obtained immediately

$$\mathrm{BW}|_{\text{spectral gap}} = \frac{(\overline{\alpha})_A}{S} \tag{A-11}$$

where S is the slope of the line segment AB, as shown Fig. 13. In practice, the slope of the line segment AB is the same as that of AD, where the solutions are usually easier to obtain. Assume that the spectral width of $(F_B - F_A)$ equals that of $(F_C - F_B)$ in (A-11).

This relation is verified using the data in [17, Figs. 4 and 5]. We get $(\alpha_x)_A = 23(1/\text{meter})$ from [17, Fig. 5] and calculate the normalized leakage constant at point A as $(\overline{\alpha})_A = (\overline{\alpha}_x^2)_A = (23/1232.7)^2 = 3.48 \times 10^{-4}$. Applying (A-10) to estimate $\overline{\beta}$ at point B, we obtain $(\overline{\beta})_B = 1 + (1/2)(\overline{\alpha})_A = 1 + (1/2) \cdot 3.48 \times 10^{-4} = 1.000174$, where $(\overline{\beta})_B$ correlates well with that shown in [17, Fig. 4].

The data from [17] are listed as follows:

$$\begin{aligned} F_A &= 58.857 \text{ GHz} \\ \left(\overline{\beta}\right)_A &= 1.0 \\ F_B &= 58.864 \text{ GHz} \\ \left(\overline{\beta}\right)_B &= 1.00017 \\ F_C &= 58.871 \text{ GHz} \\ \left(\overline{\beta}\right)_C &= 1.0 \\ F_D &= 58.850 \text{ GHz} \\ \left(\overline{\beta}\right)_D &= 0.99983. \end{aligned}$$

The spectral gap of [17, Fig. 4] is 14 MHz. Applying (A-11) allows us to calculate the bandwidth of the spectral gap

$$\begin{aligned} \mathrm{BW}|_{\text{spectral gap}} &= 3.48 \cdot 10^{-4} \frac{(58.857 - 58.850) \cdot \text{GHz}}{1.0 - 0.99983} \\ &\approx 14 \text{ MHz}. \end{aligned}$$

The estimated value is in excellent agreement with the bandwidth of the case study in [17].

In our case study, the normalized phase constant and the leaky constant at points A and D (see Fig. 13) are listed in Table I. Applying (A-11) allows us to obtain the bandwidth of the spectral gap

$$\begin{aligned} \mathrm{BW}|_{\text{spectral gap}} &= 0.23 \cdot 10^{-6} \frac{(7.22896 - 7.22880) \cdot \text{GHz}}{1.0 - 0.9999962} \\ &\approx 10 \text{ kHz}. \end{aligned}$$

REFERENCES

[1] D. Ngheim, J. T. Williams, D. R. Jackson, and A. A. Oliner, "Leakage of the dominant mode on stripline with a small gap," *IEEE Trans. Microwave Theory Tech.*, vol. 43, pp. 2549–2556, Nov. 1995.

[2] ——, "Existence of a leaky dominant mode on microstrip line with an isotropic substrate: Theory and measurements," *IEEE Trans. Microwave Theory Tech.*, vol. 44, pp. 1710–1715, Oct. 1995.

[3] ——, "The effect of substrate anisotropy on the dominant-mode leakage from stripline with an airgap," *IEEE Trans. Microwave Theory Tech.*, vol. 43, pp. 2831–2838, Dec. 1995.

[4] N. K. Das, "Power leakage, characteristic impedance, and leakage-transition behavior of finite-length stub sections of leaky printed transmission lines," *IEEE Trans. Microwave Theory Tech.*, vol. 44, pp. 526–536, Apr. 1996.

[5] ——, "Methods of suppression or avoidance of parallel-plate power leakage from conductor-backed transmission lines," *IEEE Trans. Microwave Theory Tech.*, vol. 44, pp. 169–181, Feb. 1996.

[6] M. Tsuji and H. Shigesawa, "Packaging of printed-circuit lines: A dangerous cause for narrow pulse distortion," *IEEE Trans. Microwave Theory Tech.*, vol. 42, pp. 1784–1790, Sept. 1994.

[7] J.-W. Sheen, T.-L. Chen, and Y.-D. Lin, "Mode-coupling phenomena of the even mode on microstrip line," in *IEEE MTT-S Int. Microwave Symp. Dig.*, vol. 3, June 1998, pp. 651–654.

[8] W. Menzel, "A new traveling wave antenna in microstrip," *Arch. Elektr. Ubertragung*, pp. 137–140, Apr. 1979.

[9] J. Chou and C. K. C. Tzuang, "Oscillator type active integrated antenna—The leaky-mode approach," *IEEE Trans. Microwave Theory Tech.*, vol. 44, pp. 2265–2272, Dec. 1996.

[10] C. C. Lin and C. K. C. Tzuang, "Bound-mode resonance improving the input matching of dual-mode leaky guiding structure," *IEEE Microwave Guided Wave Lett.*, vol. 8, pp. 415–420, Dec. 1998.

[11] Y.-D. Lin, J.-W. Sheen, and C. K. C. Tzuang, "Analysis and design of feeding structures for microstrip leaky wave antenna," *IEEE Trans. Microwave Theory Tech.*, vol. 44, pp. 2265–2272, Sept. 1996.

[12] F. Mesa, C. D. Nallo, and D. R. Jackson, "The theory of surface-wave and space-wave leaky-mode excitation on microstrip lines," *IEEE Trans. Microwave Theory Tech.*, vol. 47, pp. 207–215, Feb. 1999.

[13] ——, "Excitation of leaky modes on multilayer stripline structures," *IEEE Trans. Microwave Theory Tech.*, vol. 46, pp. 1062–1071, Aug. 1998.

[14] K. C. Gupta, "Computer-aided design of microwave circuits," in *Microwave Network Representation*. Norwood, MA: Artech House, 1981, ch. 2.

[15] T. Itoh, "Spectral domain immitance approach for dispersion characteristics of generalized printed transmission lines," *IEEE Trans. Microwave Theory Tech.*, vol. MTT-28, pp. 733–736, July 1980.

[16] J. R. Brews, "Characteristic impedance of microstrip lines," *IEEE Trans. Microwave Theory Tech.*, vol. MTT-35, pp. 30–34, Jan. 1987.

[17] P. Lampariello, F. Frezza, and A. A. Oliner, "The transition region between bound-wave and leaky-wave ranges for a partially dielectric-loaded open guiding structure," *IEEE Trans. Microwave Theory Tech.*, vol. 38, pp. 1831–1836, Dec. 1990.

[18] M. Tsuji, H. Shigesawa, H. Sannomiya, and A. A. Oliner, "The spectral gap when power leaks into more than one type of surface wave on printed-circuit lines," in *IEEE MTT-S Int. Microwave Symp. Dig.*, vol. 2, 1997, pp. 483–486.

[19] K. S. Lee, "Microstrip line leaky antenna," Ph.D. dissertation, Dept. Electrophys., Polytech. Univ., Brooklyn, NY, 1986.

[20] M. L. Majewki, R. W. Rose, and J. R. Scott, "Modeling and characterization of microstrip-to-coaxial transitions," *IEEE Trans. Microwave Theory Tech.*, vol. MTT-29, pp. 799–805, Aug. 1981.

[21] M. Caulton, J. Hughes, and J. Sohol, "Measurements on the properties of microstrip transmission line for MICs," *RCA Rev.*, vol. 27, pp. 377–391, Sept. 1966.
[22] Jackson, *Classical Electrodynamics*, 2nd ed. New York: Wiley, 1975, pp. 301–302.
[23] A. A. Oliner, "Leakage from higher modes on microstrip line with application to antennas," *Radio Sci.*, vol. 22, pp. 907–912, Nov. 1987.
[24] K. A. Michalski and D. Zheng, "On the leaky modes of open microstrip lines," *Microwave Opt. Technol. Lett.*, vol. 2, pp. 6–8, Jan. 1989.
[25] J. S. Bagby, C.-H. Lee, D. P. Nyquist, and Y. Yuan, "Identification of propagation regimes on integrated microstrip transmission lines," *IEEE Trans. Microwave Theory Tech.*, vol. 41, pp. 1887–1894, Nov. 1993.
[26] D. K. Cheng, *Field and Wave Electromagnetics*, 2nd ed. Reading, MA: Addison-Wesley, 1989, ch. 9-4.
[27] W. C. Chew, *Waves and Fields Inhomogeneous Media*. New York: IEEE Press, 1995, ch. 2.
[28] C.-T. Tai, *Dyadic Green Function in Electromagnetic Theory*, 2nd ed. New York: IEEE Press, 1994.

Shyue-Dar Chen (S'96–M'99) was born in Taiwan, R.O.C., on August 11, 1958. He received the B.S. degree in physics from the National Taiwan Normal University, Taipei, Taiwan, R.O.C., in 1981, the M.S. degree from Tsing Hua University, Hsinchu, Taiwan, R.O.C., in 1986, and is currently working toward the Ph.D. degree in communication engineering at the National Chiao Tuang University, Hsinchu, Taiwan, R.O.C.

From 1986 to 1996, he was with the Chung Shang Institute of Science and Technology, Lung-Tan, Taiwan, R.O.C., where he was involved with the design and development of hardware for microwave systems. His research interests are mainly in the area of computational electromagnetics and propagation of guiding structures.

Ching-Kuang C. Tzuang (S'80–M'83–SM'84–F'97) received the B.S. degree in electronic engineering from the National Chiao Tung University, Hsinchu, Taiwan, R.O.C., in 1977, the M.S. degree from the University of California at Los Angeles, in 1980, and the Ph.D. degree in electrical engineering from the University of Texas at Austin, in 1986.

From 1981 to 1984, he was with TRW, Redondo Beach, CA, where he was involved with analog and digital monolithic microwave integrated circuits. Since 1986, he has been with the Institute of Communication Engineering, National Chiao Tung University. His research activities involve the design and development of millimeter-wave and microwave active and passive circuits and the field theory analysis and design of various complex waveguiding structures and large array antennas. To date, 53 M.S. and 14 Ph.D. degree students have graduated under his supervision.

Dr. Tzuang helped form the IEEE Microwave Theory and Techniques Society (IEEE MTT-S), Taipei Chapter, and served as its secretary, vice chairman, and chairman in 1988, 1989, and 1990, respectively. He has served on the Asia–Pacific Microwave Conference International Steering Committee, where he has served as the international liaison officer representing the Taipei Chapter since 1994.